Iran J Sci Technol Trans Mech Eng (2016) 40:169–180
DOI 10.1007/s40997-016-0019-3

RESEARCH PAPER

Dynamic Performance Evaluation of Serial and Parallel RPR Manipulators with Flexible Intermediate Links

Saeed Ebrahimi[1] · **Amirhossein Eshaghiyeh-Firoozabadi**[1]

Received: 9 May 2015 / Accepted: 21 December 2015 / Published online: 28 June 2016

Abstract This paper presents a comprehensive study of the workspace, dynamic characteristics and accuracy of three planar flexible manipulators with 3-RPR, 2-RPR and 1-RPR structures moving at high speed. A geometrical procedure is employed to obtain the workspaces of the manipulators. The flexible intermediate links are modeled as the Euler–Bernoulli beams with fixed-free boundary conditions based on the assumed mode method. Using the Lagrange multipliers, a generalized set of differential algebraic equations of motion is developed for the planar RPR manipulators. Three moving constraints, which are obtained from an inverse kinematics analysis and applied to the actuated base joints, impose the end-effector to follow a high-speed circular motion as the desired trajectory. From this analysis, the dynamic performance of 1-RPR flexible serial manipulator and 2-RPR and 3-RPR flexible parallel manipulators in tracking a desired trajectory is evaluated. Based on the results, it is concluded that, in addition to the specific structure of the manipulator, the accuracy generally depends on the operation conditions. The results contest the general assertion which claims that parallel manipulators have more accuracy and stiffness than serial counterparts.

Keywords Comparative study of manipulators · Trajectory tracking · Serial and parallel manipulators · Flexible manipulators

✉ Saeed Ebrahimi
ebrahimi@yazd.ac.ir

Amirhossein Eshaghiyeh-Firoozabadi
isaac_iut2004@yahoo.com

[1] Department of Mechanical Engineering, Yazd University, Yazd, Iran

1 Introduction

During the past few years, the application of parallel manipulators has gained considerable attention due to their advantages over serial manipulators. In sensitive industries such as precision machining and robot-assisted surgery, any deviation and vibration of the end-effector can make undesired effects. Structural flexibility of the components such as joints and links is the major source of undesired deflections. At high operational speeds, inertial forces of moving components can become very large, leading to considerable deflections of the light links which in turn impose deviation of the end-effector from a desired trajectory. The cumulative effect of these deformations decreases the demanded level of accuracy. This important issue can be more challenging when dealing with flexible serial manipulators for some applications. In the past decades, considerable effort has been devoted to the dynamic analysis of flexible manipulators for the study of their accuracy. Dwivedy and Eberhard (2006) presented a survey of the literature related to dynamic analysis of flexible manipulators. They described different modeling techniques for flexible manipulators and carried out a good literature survey related to the modeling of single, two and multi-flexible link manipulators and also flexible joint manipulators.

Pandilove and Dukovski (2014) have compared the characteristics between serial and parallel manipulators. Patel and George (2012) have listed several advantages of parallel manipulators over their serial counterparts. Among all, great load carrying capacity, low inertia, higher stiffness, reduced errors and higher accuracy of parallel manipulators can be mentioned. On the other hand, serial manipulators have larger workspace, fewer constraints and simpler equations. Among the advantages of parallel

manipulators, the accuracy is challenging. Wavering (1999) gives an overview of history and current status of research in parallel kinematic machines at NIST. Song et al. (1999) derived the inverse and forward kinematic models to analyze and enhance the performance of a hexapod machine with parallel kinematic structure. They modeled the error of the parallel kinematic machine and compensated it.

On one hand, it is widely claimed in the literature that parallel manipulators have intrinsically more stiffness and accuracy than serial manipulators (see, e.g., (Guan et al. 2004; Rauf et al. 2004; Merlet 2006; Le et al. 2013; Williams and Joshi 1999)). On the other hand, the simulations which confirm this assertion have not been properly addressed. Only Briot and Bonev (2007) have pointed out that there is no simple answer to this question of superiority. They have tried to address this void statement and confirm that parallel robots are generally less sensitive to input errors than serial robots by comparing the kinematic accuracy of two pairs of serial–parallel 2-DOF planar robots. However, their comparison is too limited to draw any general conclusions. Therefore, it is very important to study the possibility of achieving less accuracy when using parallel manipulators instead of serial manipulators for some certain conditions. The main goal of this paper is to address this critical issue.

Comparative study of parallel manipulators has been considered by some researchers for performance evaluation. Among the earliest studies on this issue, Tsai and Joshi (2001) conducted a comparative study of the well-conditioned workspace, stiffness and inertia properties of four 3-DOF translational parallel manipulators. Wu et al. (2010, 2011) compared the dynamic performances of three planar 3-DOF parallel manipulators with 4-RRR, 3-RRR and 2-RRR structures and showed that the 2-RRR parallel manipulator has the worst dynamic performance. Also, in (Wu et al. 2013) they compared the performance of planar 3-DOF parallel manipulators with one and two additional branches. Some of the other studies on the dynamics of parallel manipulators are presented in (Zhang et al. 2012; Wu et al. 2010; Zhao and Gao 2009).

Binaud et al. (2011) compared two non-degenerate and two degenerate 3-RPR planar parallel manipulators with regard to their dexterity, workspace size and sensitivity. The authors of (El-Khasawneh and Alazzam 2013) carried out the forward and inverse kinematic and dynamic analysis of this manipulator. Staicu (2009) established recursive matrix relations for kinematics and dynamics and presented power requirement comparison on its dynamics. He also studied the inverse dynamics of this manipulator (Staicu 2009). The internal joint forces are considered in dynamics of a 3-PRP planar parallel robot (Staicu and Chablat 2012) and a 3-RRR parallel manipulator (Staicu 2013). In another work (Staicu 2009), the power requirement comparison in 3-RPR planar parallel robot dynamics is studied. The principle of virtual work in the inverse dynamic problem was used.

Briot and Bonev (2008) presented a detailed study of the local maximum orientation and position errors occurring in 3-RPR and 3-PRR planar parallel robots subjected to errors in the inputs. The authors of (Williams and Joshi 1999) described the design, construction and control of a planar 3-RPR parallel manipulator by including forward pose kinematics but did not consider dynamic modeling strategy. Bonev et al. (2003) described several types of singular configurations by studying the direct kinematics model of a 3-RPR planar parallel robot with actuated base joints. Recursive matrix relations for the kinematic analysis of this robot with pneumatic or hydraulic actuators were established in (Staicu et al. 2007). In another study (Briot et al. 2008), the kinematic geometry of the general 3-RPR planar parallel robots with actuated base joints was studied. Viliani et al. (2012) investigated vibration analysis of a 3-RPR parallel mechanism with flexible intermediate links. Sudhakar and Srinvas (2013) presented an analytical approach for calculating the stiffness matrix of 3-RPR parallel manipulator.

Pashkevich et al. (2009) presented a new stiffness modeling method for over-constrained parallel manipulators with flexible links and compliant actuating joints. The advantages of the developed technique are confirmed by application examples, which deal with comparative stiffness analysis of two translational parallel manipulators of 3-PUU and 3-PRP architectures. Niaritsiry et al. (2004) considered a 3 DOF in translation of high-precision parallel manipulator having flexure hinges for the purpose of studying its performances in terms of absolute positioning accuracy in presence of different sources of inaccuracy. Piras et al. (2004) presented a dynamic finite element analysis of a planar fully parallel robot with flexible links. They showed that for a given high-speed motion, the configuration of the mechanism has a significant influence on the nature of the resultant elastic vibrations. Kang and Mills (2002) developed the fully coupled equations of motion of a 3-PRR planar parallel manipulator by considering structural flexibility of the intermediate links, using the Lagrange multipliers method. For evaluating the coupling effects between the degree-of-freedom motions of six-degree-of-freedom parallel manipulators, a method has been presented in Ogbobe et al. (2011). This approach is based on singular-value decomposition to the properties of the joint space inverse mass matrix. Seifried et al. (2013) presented the feedforward control designs based on inverse models and applied to serial and parallel flexible manipulators. Thereby, for a given system output the inverse model provides the control input for exact reproduction of

the desired output trajectory and the trajectories of the generalized coordinates.

A dynamic model of a 3-RPR planar parallel manipulator has been presented in our preliminary work (Firoozabadi et al. 2015). In this paper, we intend to investigate the accuracy and stiffness of the flexible parallel manipulators versus serial manipulators in high speeds. For this purpose, three planar manipulators are selected with 3-RPR and 2-RPR parallel structures and 1-RPR serial structure. The flexibility of the manipulators is concentrated in intermediate links, as the rest of the structure is mechanically far stiffer. The structural flexibility of the intermediate links is modeled by the assumed mode method considering three mode shapes. The dynamic model of 3-RPR, 2-RPR and 1-RPR manipulators with flexible intermediate links is developed. The flexible intermediate links are modeled as the Euler–Bernoulli beams with fixed-free boundary conditions. Using the Lagrange multipliers, a generalized set of differential algebraic equations (DAEs) of motion is developed. A high-speed motion of the end-effector is selected to compare the deviations from the desired trajectory due to deformations of the links.

2 Architecture of the 3-RPR, 2-RPR and 1-RPR Manipulators

The main parallel manipulator presented in this work is categorized as a 3-RPR type, as shown in 3D and 2D views in Fig. 1, respectively. The manipulator is planar, and the motion of the end-effector is two dimensional. This manipulator comprises three symmetric RPR chains, each of which consists of a revolute joint (R), then a prismatic joint (P) and again a revolute joint (R), respectively. It is composed of two triangular platforms: the moving platform ($C_1C_2C_3$) and the fix platform ($A_1A_2A_3$) which are equilateral triangles, as shown in Fig. 1. The end-effector is installed on the mass center point P of the moving platform ($C_1C_2C_3$). The gravity is perpendicular to the manipulator plane.

On the fixed platform ($A_1A_2A_3$), there are three revolving cylinders (A_iB_i) in which three moving sliders reciprocate and provide linear actuations for each leg of the flexible intermediate link. So, each prismatic joint at point B_i ($i = 1, 2, 3$) is connected to the platform through a flexible link (B_iC_i) with length l. The other end of the links, C_i, $i = 1, 2, 3$, is connected to the moving platform with revolute joints. As can be perceived from the figure, two local coordinates are defined for each flexible link. Coordinate x_i is assumed to be in the direction of the ith undeformed intermediate link, and coordinate $w_i(x)$ is defined as the bending deflection of ith intermediate link from its rigid configuration. The origin O of the fixed coordinate frame, which has been hidden behind the moving platform, is located at the geometrical center point of the triangle $A_1A_2A_3$. The rotation angle of each rigid link A_iB_i is specified with θ_i. The variable distance due to the actuation of prismatic joint between points B_i and A_i is defined as ρ_i. The manipulators with structures 2-RPR and 1-RPR are shown in Figs. 2 and 3. Table 1 reports the necessary parameters of the manipulators.

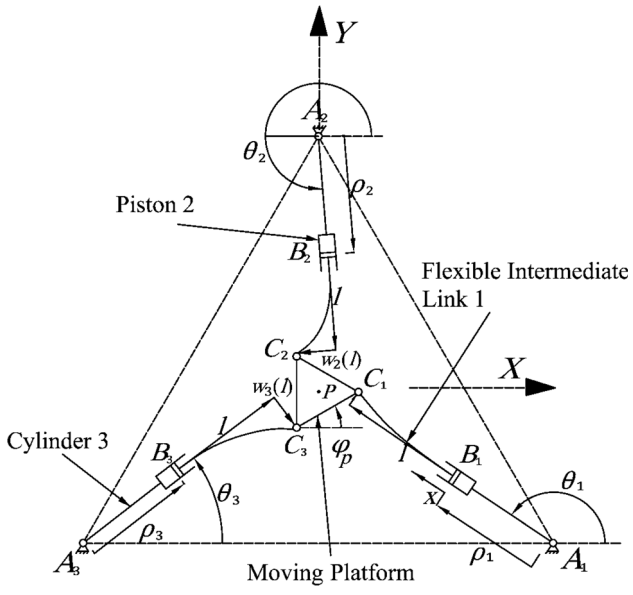

Fig. 1 Coordinates system of the proposed 3-RPR manipulator

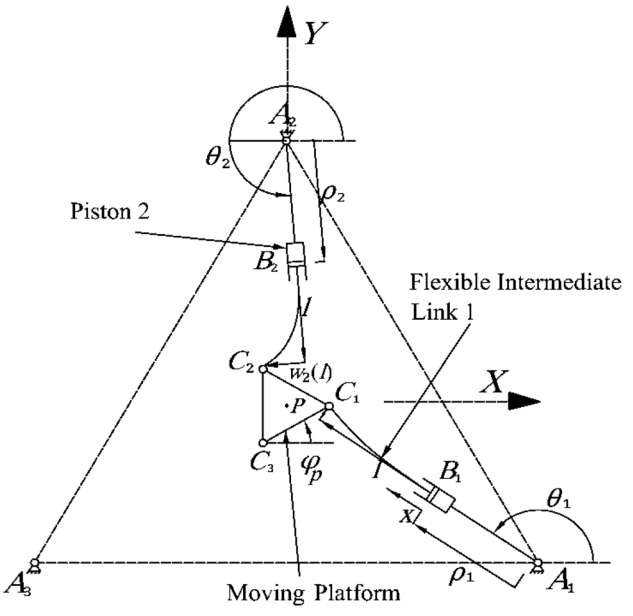

Fig. 2 Coordinates system of the proposed 2-RPR manipulator

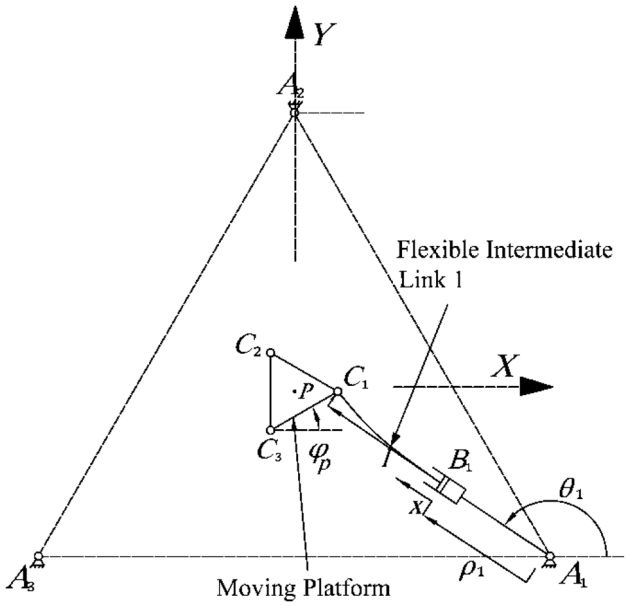

Fig. 3 Coordinates system of the proposed 1-RPR manipulator

3 Workspaces of the Manipulators

In this section, the reachable workspaces of the manipulators (for the end-effector center point P) assuming rigid links are obtained. We describe a procedure for this purpose which utilizes simple geometrical rules. For the 3-RPR manipulator, the reachable workspace is the common area between reachable zones by the three RPR chains, as shown in Fig. 4.

The reachable area for the end-effector from each RPR chain, ignoring the other RPR chains, is the common area between two circles. Each smaller circle (inner circle) is the trajectory of the end-effector when $\rho_i = 0$ and $\varphi_p = 0$, ignoring the other RPR chains. The radius of the smaller circle is obtained as

$$\rho_i = 0 \rightarrow A_iC_i = A_iB_i = l \rightarrow R_1 = A_iC_i + C_iP = l + b\sqrt{3}/3 \quad (1)$$

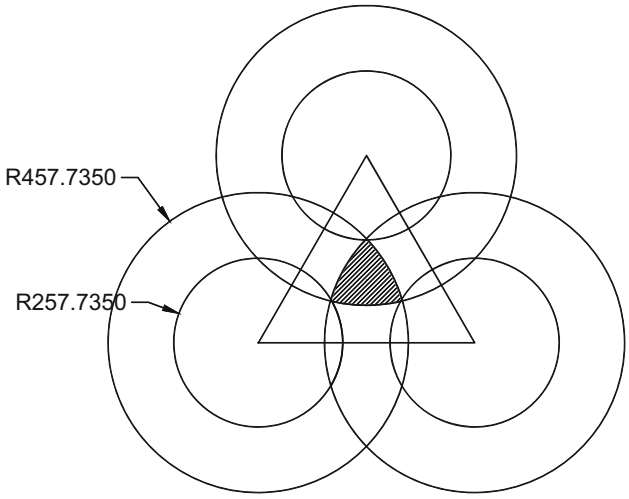

Fig. 4 Reachable workspace of the 3-RPR manipulator (all dimensions are in mm)

where b is the side length of moving platform and R_1 is the radius of the smaller circle which is the minimum distance between the end-effector and A_i joint assuming $\varphi_p = 0$. Every larger circle (outer circle) for each RPR chain is the trajectory of the end-effector when $\rho_i = B_iC_i = l$ and $\varphi_p = 0$, ignoring the other RPR chains. The radius of larger circle is obtained as

$$\rho_i = B_iC_i = l \rightarrow A_iC_i = A_iB_i + B_iC_i = 2l \rightarrow R_2 = A_iC_i + C_iP = 2l + b\sqrt{3}/3 \quad (2)$$

where R_2 is the radius of the larger circle which is the maximum distance between the end-effector and A_i joint assuming $\varphi_p = 0$. By substituting the parameters from Table 1 into Eqs. (1) and (2), we have

$$R_1 = A_iB_i + C_iP = 200 + 100 \times \sqrt{3}/3 = 257.735\,\text{mm} \quad (3)$$

$$R_2 = A_iB_i + B_iC_i + C_iP = 200 + 200 + 100 \times \sqrt{3}/3 = 457.735\ \text{mm} \quad (4)$$

Table 1 Planar n-RPR manipulators parameters ($n = 1, 2, 3$)

Moving platform	Side length ($C_iC_{i+1} = b$)	100 mm
	Mass	0.5 kg
Flexible intermediate links	Length ($B_iC_i = l$)	200 mm
	Cross-sectional diameter	10 mm
	Density	2772 kg/m^3
	Young's modulus	73 GPa
Cylinders (rigid links)	Motion course amplitude (A_iB_i)	200 mm
	Inner diameter	20 mm
	Outer diameter	24 mm
	Mass density	7800 kg/m^3
Fixed platform	Side length (A_iA_{i+1})	660 mm

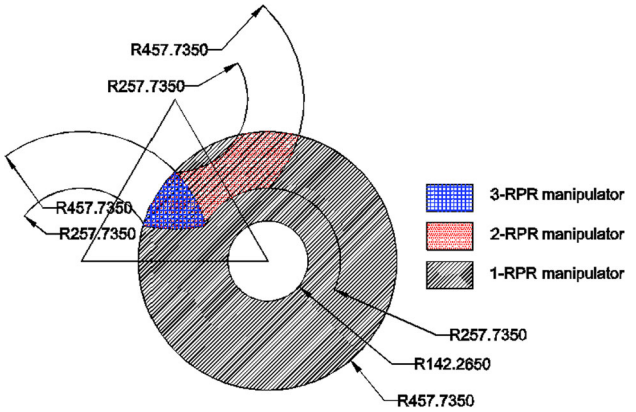

Fig. 5 Reachable workspaces of the rigid 3-RPR, 2-RPR and 1-RPR manipulators (all dimensions are in mm)

By following this procedure, one can obtain the workspaces of the 2-RPR and 1-RPR manipulators as shown in Fig. 5. Note that in the 1-RPR manipulator, when $\rho_i = 0$, the moving platform can rotate around the C_i joint with a much larger angle, due to absence of the other RPR chain constraints. So, the radius of the smaller circle for this manipulator is written as

$$R_3 = A_iB_i - C_iP = l - b\sqrt{3}/3 = 200 - 100 \times \sqrt{3}\Big/3 = 142.265 \text{ mm} \quad (5)$$

Figure 5 illustrates the workspace of the 1-RPR manipulator including the workspaces of the 2-RPR and 3-RPR manipulators, and also the workspace of the 2-RPR manipulator which includes the workspace of the 3-RPR manipulator. As a result, the larger workspace of the serial 1-RPR manipulator compared to the parallel 2-RPR and 3-RPR manipulators is confirmed.

4 Flexibility Modeling of the Intermediate Links with the Assumed Mode Method

In this work, the assumed mode method (AMM) is employed to model the structural flexibility of the intermediate links. Each intermediate link, B_iC_i, of the three manipulators is modeled as an Euler–Bernoulli beam because the length of each link is much longer than its cross-sectional diameter. Study on the flexibility of the joints is not discussed in this work, and therefore, they are assumed rigid. Also, the platform $C_1C_2C_3$ and links A_iB_i are assumed rigid because they are designed and built to be much stiffer than the intermediate links B_iC_i. Based on the AMM, the transverse deflections of the links are modeled by an infinite number of separable harmonic modes. Since only the first few modes dominate the dynamics, the modes are truncated to a finite number of modal series. According to the formulation of the AMM, bending deformation of the ith flexible link of the RPR manipulators can be expressed as

$$w_i(x,t) = \sum_{j=1}^{r} \eta_{ij}(t)\psi_j(x), \quad i = 1, \ldots, n \quad (6)$$

where $w_i(x, t)$ is the bending deflection of the flexible link that varies along the link length with time, $\psi_j(x)$ is the mode shape function and $\eta_{ij}(t)$ is the time-varying mode amplitude. Index i is the link number, j is the mode shape number and r is the number of selected assumed modes for modeling of the link flexibility. Scalar n for the 3-RPR, 2-RPR and 1-RPR manipulators is three, two and one, respectively. Vector of the generalized flexible coordinates $\bar{\boldsymbol{\eta}}$ with dimension $nr \times 1$ ($n = 1, 2, 3$) is defined as

$$\bar{\boldsymbol{\eta}} = [\eta_{11}, \ldots, \eta_{1r}, \ldots, \eta_{n1}, \ldots, \eta_{nr}]^T \quad (7)$$

where η_{ij} with $i = 1,\ldots, n$ and $j = 1, 2,\ldots, r$ denotes the jth mode coordinate of the ith flexible link of the n-RPR manipulator.

The flexible intermediate links are treated as rigid in the longitudinal direction since the axial stiffness of intermediate links is much higher than the lateral stiffness. The fixed-free boundary conditions are selected for the intermediate links. Due to the rigidity of the prismatic joints, the slope and deflection of the flexible links at point B_i are zero and so, fixed boundary condition is adopted here. The boundary condition at the endpoint C_i of the flexible links was chosen as free to transmit the effects of the links flexibility to the moving platform. For the fixed-free boundary conditions, the mode shape function $\psi_j(\xi)$ that is presented in (Rao 2007) can be easily developed in dimensionless form as

$$\psi_j(\xi) = \left[\left(\cos\alpha_j\xi - \cosh\alpha_j\xi\right) - \frac{\cos\alpha_j + \cosh\alpha_j}{\sin\alpha_j + \sinh\alpha_j}\left(\sin\alpha_j\xi - \sinh\alpha_j\xi\right)\right] \quad (8)$$

Here, $\xi = \frac{x}{l}$, $0 \le \xi \le 1$, where x is the distance from B_i to an arbitrary point on the ith flexible link, and l is the link length. The parameter α_i is obtained from the solution of the following frequency equation

$$\cos\alpha_j \cosh\alpha_j + 1 = 0 \quad j = 1, 2, \ldots, r \quad (9)$$

where, for example, α_1 to α_4 are written as

$$\alpha_1 = 1.875104069,\ \alpha_2 = 4.694091133,\ \alpha_3 = 7.854757438,\ \alpha_4 = 10.99554073 \quad (10)$$

5 Equations of Motion of the Manipulators

In this section, the fully coupled equations of motion of the n-RPR parallel manipulators with flexible intermediate links using the Lagrange multipliers method are presented.

These equations include dynamic equations and kinematic constraint equations. For deriving the equations, the rigid body and elastic motions are incorporated as a set of generalized coordinates.

5.1 Kinetic Energy

The total kinetic energy of the manipulators include the kinetic energies of the rigid cylinders (A_iB_i), the flexible intermediate links (B_iC_i) and the moving platform. The kinetic energy of the rigid cylinders A_iB_i is given as

$$T_C = \sum_{i=1}^{n} \frac{1}{2} I_c \dot{\theta}_i^2 \tag{11}$$

where n is three, two and one for the 3-RPR, 2-RPR and 1-RPR manipulators, respectively, I_c is the mass moment of inertia of the ith rigid cylinder about its rotating axis at point A_i, and $\dot{\theta}_i$ is the angular velocity of this link.

The kinetic energy of the flexible intermediate links B_iC_i is expressed as

$$T_L = \sum_{i=1}^{n} \frac{1}{2} \int_0^l \rho_A \left[\dot{\rho}_i^2 + \left((x + \rho_i)\dot{\theta}_i + \dot{w}_i(x) \right)^2 \right] \mathrm{d}x \tag{12}$$

where ρ_A is the mass per unit length of each flexible link with mass m, $\dot{w}_i(x)$ is the time derivative of bending deformation, and $\dot{\rho}_i$ is the linear velocity of flexible link i in the direction of its undeformed configuration. Finally, the kinetic energy of the platform is expressed as

$$T_P = \frac{1}{2} m_{\mathrm{p}} (\dot{x}_{\mathrm{p}}^2 + \dot{y}_{\mathrm{p}}^2) + \frac{1}{2} I_{\mathrm{p}} \dot{\varphi}_{\mathrm{p}}^2 \tag{13}$$

where I_{p} is the mass moment of inertia of the platform around the center point P, m_{p} is the platform mass, $\dot{x}_{\mathrm{p}}$ and $\dot{y}_{\mathrm{p}}$ are the linear velocities along the X and Y axes, respectively, and $\dot{\varphi}_{\mathrm{p}}$ is the angular velocity of the platform.

The total kinetic energy can be obtained by summing the kinetic energy of all components as

$$\begin{aligned} T = & \sum_{i=1}^{n} \frac{1}{2} I_c \dot{\theta}_i^2 + \sum_{i=1}^{n} \frac{1}{2} \int_0^l \rho_A \left[\dot{\rho}_i^2 + \left((x + \rho_i)\dot{\theta}_i + \dot{w}_i(x) \right)^2 \right] \mathrm{d}x \\ & + \frac{1}{2} m_{\mathrm{p}} (\dot{x}_{\mathrm{p}}^2 + \dot{y}_{\mathrm{p}}^2) + \frac{1}{2} I_{\mathrm{p}} \dot{\varphi}_{\mathrm{p}}^2 \end{aligned} \tag{14}$$

5.2 Potential Energy

The potential energy of a flexible manipulator system generally arises from two sources: the elastic deformation of flexible links and gravity. Gravitational force which is perpendicular to the manipulators plane, and therefore, the potential energy due to the gravity is not included here. The potential energy of the system due to the bending deflection of flexible links is given as

$$\begin{aligned} V &= \frac{1}{2} \sum_{i=1}^{n} \int_0^l EI \left(\frac{\partial^2 w_i(x)}{\partial x^2} \right)^2 \mathrm{d}x \\ &= \frac{1}{2} \sum_{i=1}^{n} \frac{\mathrm{EI}}{l^3} \int_0^1 \sum_{j=1}^{r} \eta_{ij}^2(t) (\psi_j''(\xi))^2 \mathrm{d}\xi \end{aligned} \tag{15}$$

where E and I are the elastic modulus and the second moment of area of each flexible link, respectively.

5.3 Lagrange Equations

The generalized coordinates of the manipulators with flexible links include rigid body motion generalized coordinates and flexible generalized coordinates. Rigid body motion coordinates for the n-RPR manipulator are selected as

$$\begin{aligned} & \bar{\boldsymbol{\rho}} = [\rho_1, \ldots, \rho_n]^{\mathrm{T}}, \quad \bar{\boldsymbol{\theta}} = [\theta_1, \ldots, \theta_n]^{\mathrm{T}} \text{ and} \\ & \bar{\mathbf{X}}_{\mathrm{p}} = \left[x_{\mathrm{p}}, y_{\mathrm{p}}, \varphi_{\mathrm{p}} \right]^{\mathrm{T}} \end{aligned} \tag{16}$$

where $\bar{\boldsymbol{\rho}}$ is the vector of translational coordinates of links B_iC_i, $\bar{\boldsymbol{\theta}}$ is the vector of rotational coordinates of links A_iB_i, and $\bar{\mathbf{X}}_{\mathrm{p}}$ is the vector of coordinates of the moving platform. The vector of generalized coordinates of the n-RPR manipulator can be written as $\mathbf{X} = \left[\bar{\boldsymbol{\rho}}^{\mathrm{T}}, \ \bar{\boldsymbol{\theta}}^{\mathrm{T}}, \ \bar{\mathbf{X}}_{\mathbf{p}}^{\mathrm{T}}, \ \bar{\boldsymbol{\eta}}^{\mathrm{T}} \right]^{\mathrm{T}} \in R^q$ where $q = ((2n + 3) + nr) \times 1$. These n-RPR manipulators, without considering the flexibilities, have three degrees of freedom; so the rigid body motion coordinates: $\bar{\boldsymbol{\rho}}$, $\bar{\boldsymbol{\theta}}$ and $\bar{\mathbf{X}}_{\mathrm{P}}$ are not independent and must satisfy $2n$ constraint equations. From the geometry of n chains of the n-RPR manipulator as shown in Figs. 2, 3 and 4, the constraint equations can be written as

$$\mathbf{r}_{\mathrm{OA}_i} + \mathbf{r}_{\mathrm{A}_i\mathrm{B}_i} + \mathbf{r}_{\mathrm{B}_i\mathrm{C}_i} = \mathbf{r}_{\mathrm{OP}} + \mathbf{r}_{\mathrm{PC}_i}, \qquad i = 1, \ldots, n \tag{17}$$

which upon projection along X and Y axes, $2n$ constraint equations are written as

$$\begin{aligned} \Gamma_{2i-1} \equiv & X_{Ai} + (\rho_i + l)\cos\theta_i - w_i(l)\sin\theta_i - x_{\mathrm{p}} \\ & - r_{\mathrm{PC}_i} \cos(\varphi_i + \varphi_{\mathrm{p}}) = 0, \qquad i = 1, \ldots, n \end{aligned} \tag{18}$$

$$\begin{aligned} \Gamma_{2i} \equiv & Y_{Ai} + (\rho_i + l)\sin\theta_i + w_i(l)\cos\theta_i - y_{\mathrm{p}} \\ & - r_{\mathrm{PC}i} \sin(\varphi_i + \varphi_{\mathrm{p}}) = 0, \qquad i = 1, \ldots, n \end{aligned} \tag{19}$$

where $r_{\mathrm{PC}_i} \cos(\varphi_i + \varphi_{\mathrm{p}}) = x_{\mathrm{ci}}^0$ and $r_{\mathrm{PC}_i} \sin(\varphi_i + \varphi_{\mathrm{p}}) = y_{\mathrm{ci}}^0$ specify the global X and Y coordinates of C_i, respectively, measured from the mass center of the platform, P, when φ_{p} is zero. Furthermore, as shown in Fig. 6, φ_i is the angle between r_{PC_i} and x-axis of local coordinate which can be written as $\varphi_1 = -\pi/6$, $\varphi_2 = \pi/2$ and $\varphi_3 = 7\pi/6$. Parameters X_{Ai} and Y_{Ai} are the X and Y coordinates of A_i, respectively, as shown in Figs. 1, 2 and 3. Note that the variables r_{PC_i}, φ_i, X_{Ai} and Y_{Ai} are constant.

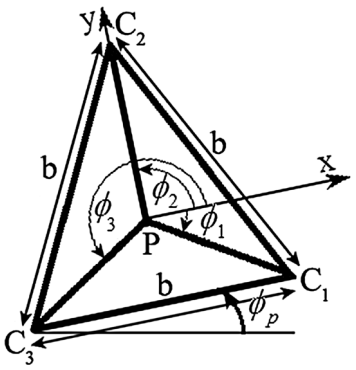

Fig. 6 Coordinates system of the moving platform

Using the Lagrange multiplier method, the dynamic equations of the manipulators with n flexible links are given as

$$\frac{\mathrm{d}}{\mathrm{d}t}\left(\frac{\partial(T-V)}{\partial \dot{X}_i}\right)-\frac{\partial(T-V)}{\partial X_i}=Q_i+\sum_{k=1}^{6}\lambda_k\frac{\partial \Gamma_k}{\partial X_i},\quad i=1,\ldots,(2n+3+nr) \tag{20}$$

where Q_i is the generalized force associated with the generalized coordinate X_i, and λ_k is the Lagrange multiplier associated with the kth constraint equation. Substituting Eqs. (14), (15), (18) and (19) into Eq. (20) results in the equations of motion of the flexible n-RPR manipulators which can be rearranged as the following differential–algebraic equations (DAEs)

$$\begin{bmatrix}\mathbf{M}_{\rho\rho} & \mathbf{0} & \mathbf{0} & \mathbf{0}\\ \mathbf{0} & \mathbf{M}_{\theta\theta} & \mathbf{0} & \mathbf{M}_{\eta\theta}^{T}\\ \mathbf{0} & \mathbf{0} & \mathbf{M}_{X_PX_P} & \mathbf{0}\\ \mathbf{0} & \mathbf{M}_{\eta\theta} & \mathbf{0} & \mathbf{M}_{\eta\eta}\end{bmatrix}\begin{bmatrix}\ddot{\bar{\boldsymbol{\rho}}}\\ \ddot{\bar{\boldsymbol{\theta}}}\\ \ddot{\bar{\mathbf{X}}}_{\mathrm{P}}\\ \ddot{\bar{\boldsymbol{\eta}}}\end{bmatrix}+\begin{bmatrix}\mathbf{K}_{\rho\rho} & \mathbf{0} & \mathbf{0} & \mathbf{0}\\ \mathbf{K}_{\theta\rho} & \mathbf{0} & \mathbf{0} & \mathbf{0}\\ \mathbf{0} & \mathbf{0} & \mathbf{0} & \mathbf{0}\\ \mathbf{0} & \mathbf{0} & \mathbf{0} & \mathbf{K}_{\eta\eta}\end{bmatrix}\begin{bmatrix}\bar{\boldsymbol{\rho}}\\ \bar{\boldsymbol{\theta}}\\ \bar{\mathbf{X}}_{\mathrm{P}}\\ \bar{\boldsymbol{\eta}}\end{bmatrix}=\begin{bmatrix}\mathbf{F}_{c\rho}\\ \mathbf{F}_{c\theta}\\ \mathbf{0}\\ \mathbf{F}_{c\eta}\end{bmatrix}+\begin{bmatrix}\mathbf{F}_{e\rho}\\ \mathbf{F}_{e\theta}\\ \mathbf{F}_{eX_P}\\ \mathbf{F}_{e\eta}\end{bmatrix}+\begin{bmatrix}\mathbf{J}_{\Gamma\rho}^{T}\\ \mathbf{J}_{\Gamma\theta}^{T}\\ \mathbf{J}_{\Gamma X_P}^{T}\\ \mathbf{J}_{\Gamma\eta}^{T}\end{bmatrix}\begin{bmatrix}\lambda_1\\ \vdots\\ \lambda_{2n}\end{bmatrix} \tag{21}$$

$$\Gamma_{2i-1}\equiv X_{Ai}+(\rho_i+l)\cos\theta_i-w_i(l)\sin\theta_i-x_{\mathrm{p}}-r_{\mathrm{PC}_i}\cos(\varphi_i+\varphi_{\mathrm{p}})=0$$

$$\Gamma_{2i}\equiv Y_{Ai}+(\rho_i+l)\sin\theta_i+w_i(l)\cos\theta_i-y_{\mathrm{p}}-r_{\mathrm{PC}i}\sin\left(\varphi_i+\varphi_{\mathrm{p}}\right)=0$$

where vectors $\mathbf{F}_{ci}$ $(i=\rho,\ \theta,\ \eta)$ include Coriolis and centrifugal forces, vectors $\mathbf{F}_{ei}(i=\rho,\ \theta,\ X_{\mathrm{p}},\eta)$ contain externally applied forces, and $\mathbf{J}_{\Gamma i}(i=\rho,\ \theta,\ X_{\mathrm{p}},\eta)$ are the constraint Jacobian matrices corresponding to the generalized coordinates. Matrices $\mathbf{M}$ and $\mathbf{K}$ are the mass and stiffness matrices, respectively. Upper index T represents transpose of matrix. The detailed expressions of the above parameters are given in the "Appendix" section.

Equation (21) is comprised of $2n+3+nr$ differential equations, $2n$ algebraic constraint equations, and $4n+3+nr$ variables equal to the number of equations. The number of degrees of freedom is $3+nr$ in the n-RPR manipulators with n flexible links, i.e., 3° of rigid body motion degree and nr degrees of elastic motion.

6 Numerical Simulation

In this section, numerical simulations for the 3-RPR and 2-RPR parallel manipulators with three and two flexible intermediate links, respectively, and 1-RPR serial manipulator with one flexible intermediate link are presented to compare the accuracy level between flexible parallel and flexible serial manipulators. Although parallel manipulators usually have higher stiffness and accuracy than serial manipulators, it will be shown that it may not be the case in some conditions. In these simulations, the first three mode shapes are selected to model the structural flexibility of the intermediate links, i.e., $r=3$.

As it can be observed, the equations of motion of the flexible n-RPR manipulators, like most of other flexible parallel manipulators, are large, highly nonlinear and complicated. Therefore, their inverse dynamic analysis is very complicated. In this paper, an easier method is employed to investigate the effects of links flexibility on the end-effector trajectory.

For simulations, a circular motion is selected as a desired trajectory for the end-effector of the moving platforms with constant orientation φ_{p}. The motion is considered with high acceleration and frequency to excite structural vibrations of the flexible linkages. The amount of deviation from the desired trajectory, due to the links flexibility, can specify the accuracy level of each manipulator.

The desired trajectory is specified as:

$$x_{\mathrm{p}}=30\cos 2\pi ft-30\,(\mathrm{mm}),\ y_{\mathrm{p}}=30\sin 2\pi ft\,(\mathrm{mm})\ \text{and}\ \varphi_{\mathrm{p}}=\frac{\pi}{4}\ \text{with}\ f=10\,\mathrm{Hz} \tag{22}$$

Since the rigid 1-RPR, 2-RPR and 3-RPR manipulators have three degrees of freedom, three moving constraints are considered to impose the required rigid body motion of the end-effector in following the desired trajectory. For this purpose, the rigid body motion coordinates ρ_1, θ_1 and φ_{p}, which are common between the three manipulators, are constrained. Based on Eqs. (18), (19) and (22), and considering that $w_i(l)=0$ in a rigid body motion, the moving constraint equations are written as

$$X_{A_1}+(\rho_1(t)+l)\cos\theta_1(t)-(30\cos(2\pi ft)-30)-r_{\mathrm{PC}_1}\cos(\varphi_1+\varphi_{\mathrm{p}}(t))=0 \tag{23}$$

$$Y_{A_1} + (\rho_1(t) + l)\sin\theta_1(t) - (30\sin(2\pi ft) - r_{PC_1}\sin(\varphi_1 + \varphi_p(t)) = 0 \quad (24)$$

$$\varphi_p(t) - \frac{\pi}{4} = 0 \quad (25)$$

Equations (23), (24) and (25) are the moving constraints which impose certain motion on the moving platform. These moving constraints do not make any change in the derivation of kinematic constraints Jacobian matrices $\mathbf{J}_{\Gamma i}(i = \rho, \theta, X_p, \eta)$. Before considering these moving constraints, components of the Jacobian matrices $\mathbf{J}_{\Gamma i}(i = \rho, \theta, X_p, \eta)$ are to be constructed using the approach explained in "Appendix" section. Indeed, the moving constraints are considered together with the system dynamic equations of motion. Corresponding to each moving constraint, a constraint force is obtained and exerted to the moving platform. As the result, the other parts of the manipulator are moved accordingly. All these steps are performed automatically in Maple within the numerical solution of the DAE.

As an important issue, it is worth mentioning that the moving constraint equations constrain the rigid body motion of the manipulators and they do not impose any constraint on the elastic deflections of the flexible links, i.e., $w_i(l) \neq 0$ which makes the end-effector deviate from the desired trajectory.

The initial values of the generalized elastic deformation $\bar{\boldsymbol{\eta}}_0$ and velocity $\dot{\bar{\boldsymbol{\eta}}}_0$ are considered to be zero. The initial positions $\bar{\boldsymbol{\rho}}_0$ and $\bar{\boldsymbol{\theta}}_0$, and velocities $\underline{\boldsymbol{\rho}}_0$ and $\underline{\boldsymbol{\theta}}_0$ of the manipulators are calculated from Eqs. (18), (19) and (22). Using the initial values, Eq. (21) is solved with Maple software by using MEBDFI solver (Modified Extended Backward-Differentiation Formula Implicit). This solver has the ability to fully solve implicit DAE systems.

Figures 7 and 8 illustrate variations in $\rho_1(t)$ and $\theta_1(t)$ which are identical for the 1-RPR, 2-RPR and 3-RPR flexible manipulators. It is prerequisite for comparison of the end-effector trajectory of the manipulators.

Figure 9 presents the elastic deformations of the flexible intermediate link B_1C_1 for the three manipulators at their endpoint C_1 connected to the moving platform. Vibrations of this point directly affect the end-effector motion. As it can be seen, the overall elastic deformation of the flexible link B_1C_1 of the 3-RPR manipulator is larger than the 2-RPR manipulator, and for the 2-RPR manipulator is larger than the 1-RPR serial manipulator.

Figure 10 illustrates the end-effector trajectories of the three flexible manipulators that deviate from the desired trajectory. The corresponding deviation magnitude (error) in following the circular trajectory is shown in Fig. 11. Maximum deviations for the 3-RPR, 2-RPR and 1-RPR manipulators are 10.003, 9.285 and 8.474 mm, respectively.

By integrating the deviations from the desired trajectory and averaging during 100 ms of the simulation, the deviation averages are obtained about 4.82, 4.43 and 3.92 mm for the 3-RPR, 2-RPR and 1-RPR manipulators, respectively. Consequently, the 1-RPR flexible serial manipulator acts stiff with higher accuracy compared to parallel 2-RPR and 3-RPR flexible manipulators. These results contest the general assertion which claims that parallel manipulators have more accuracy and stiffness than serial counterparts.

Reasons which may contribute to decrease the stiffness and accuracy from the 1-RPR flexible serial manipulator to the 3-RPR flexible parallel manipulator can be classified as:

1. The total mass of the manipulators increases from the 1-RPR manipulator to the 3-RPR manipulator due to increasing the number of components which increases

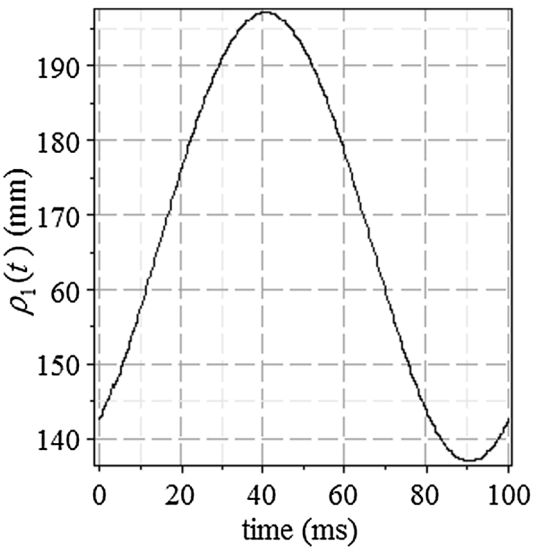

Fig. 7 Variations in $\rho_1(t)$ for the 1-RPR, 2-RPR and 3-RPR flexible manipulator

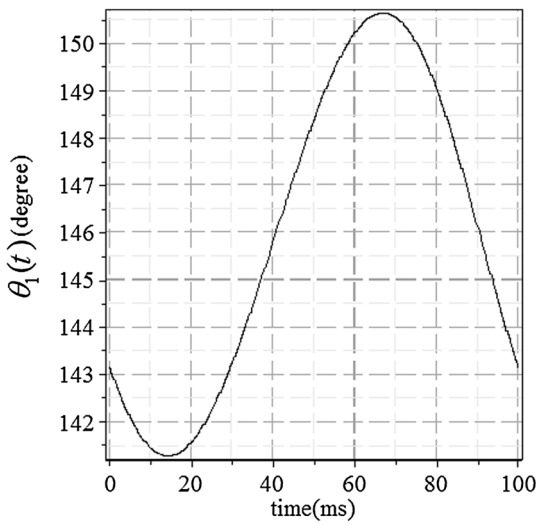

Fig. 8 Variations in $\theta_1(t)$ for the 1-RPR, 2-RPR and 3-RPR flexible manipulator

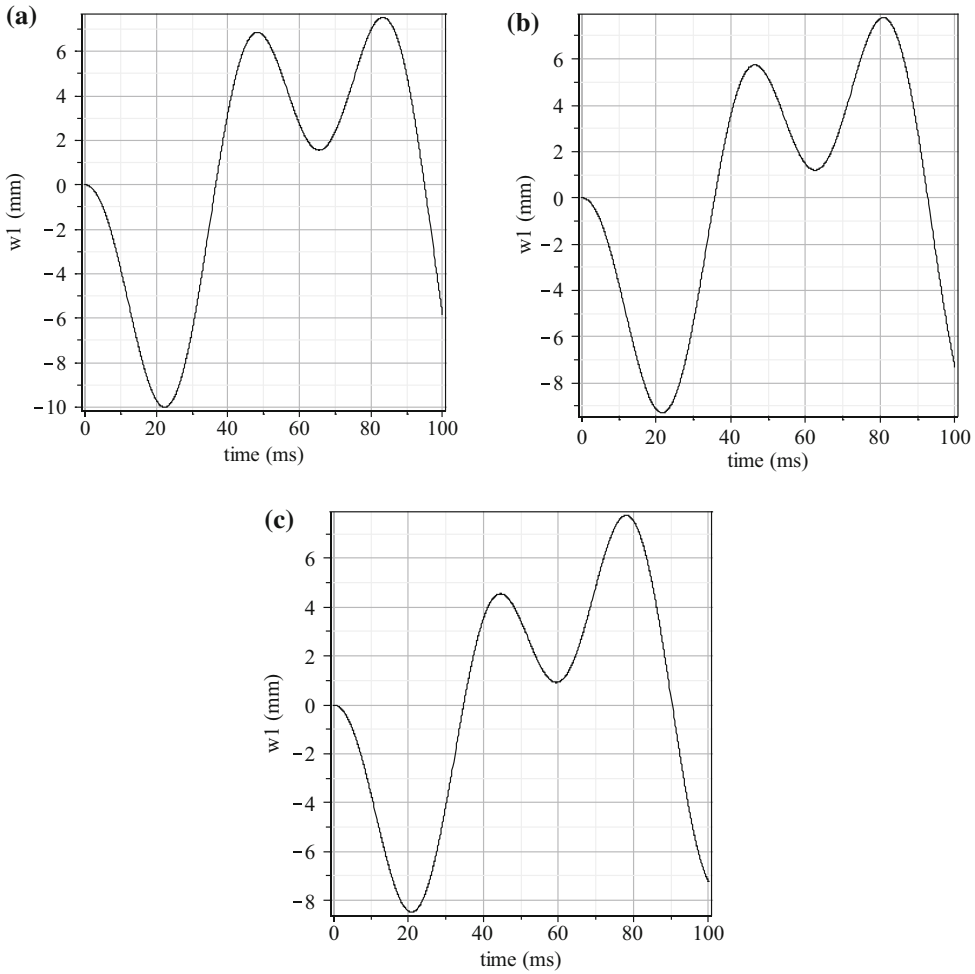

Fig. 9 Endpoint C_1 deformation of the flexible link B_1C_1 of the three manipulators. **a** 3-RPR flexible parallel manipulator, **b** 2-RPR flexible parallel manipulator, **c** 1-RPR flexible serial manipulator

the inertial forces and the deformations of the flexible links.

2. The degrees of freedom of the elastic motion of the flexible manipulators increase from the 1-RPR manipulator to the 3-RPR manipulator.
3. In very flexible serial manipulators, the deformations of flexible links are added cumulatively, while in the parallel manipulators they are averaged. However, here in these manipulators, in which only intermediate links are considered flexible, this situation is not the case.

7 Conclusion

This work investigates the effects of links flexibility on the rigid body motion of the moving platform of the 3-RPR and 2-RPR parallel manipulators and 1-RPR serial manipulator with flexible intermediate links moving at high speeds. A geometrical procedure was employed to obtain the workspaces of the manipulators. The equations of motion, including the differential algebraic equations and algebraic constraint equations, for the three flexible manipulators were developed by using the Lagrange multipliers method. The structural flexibility of the intermediate links was modeled by the assumed mode method considering three mode shapes. Three moving kinematic constrains, obtained from an inverse kinematics analysis and applied to the actuated base joints, imposed the end-effector to follow a high-speed circular motion as the desired trajectory. The simulation results illustrated that the stiffness and accuracy decrease from the 1-RPR serial manipulator to the 3-RPR parallel manipulator. These results disagree with the general assertion which claims that parallel manipulators have more accuracy and stiffness than serial counterparts.

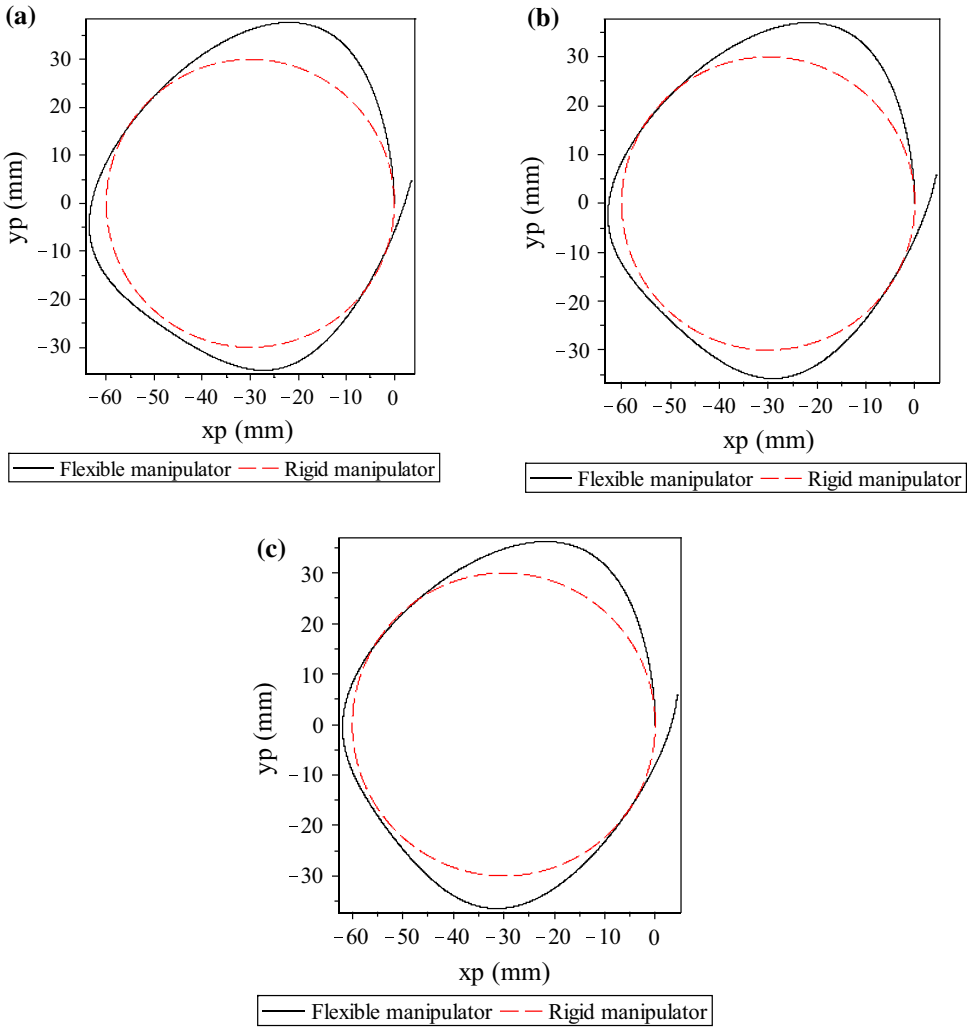

Fig. 10 Trajectory of the end-effector of the flexible manipulators. **a** 3-RPR parallel manipulator, **b** 2-RPR parallel manipulator, **c** 1-RPR serial manipulator

Appendix

Mass matrix:

$$\mathbf{M}_{\rho\rho} = m\begin{bmatrix} 1 & \cdots & 0 \\ \vdots & \ddots & \vdots \\ 0 & \cdots & 1 \end{bmatrix} \in R^{n\times n},$$

$$\mathbf{M}_{\theta\theta} = \left(I_c + \frac{ml^2}{3}\right)\begin{bmatrix} 1 & \cdots & 0 \\ \vdots & \ddots & \vdots \\ 0 & \cdots & 1 \end{bmatrix} + m\begin{bmatrix} l\rho_1 + \rho_1^2 & \cdots & 0 \\ \vdots & \ddots & \vdots \\ 0 & \cdots & l\rho_n + \rho_n^2 \end{bmatrix} \in R^{n\times n}$$

$$\mathbf{M}_{X_pX_p} = \begin{bmatrix} m_p & 0 & 0 \\ 0 & m_p & 0 \\ 0 & 0 & I_p \end{bmatrix}, \quad \mathbf{M}_{\eta\eta} = m\begin{bmatrix} \hat{\mathbf{M}} & 0 & 0 \\ 0 & \ddots & 0 \\ 0 & 0 & \hat{\mathbf{M}} \end{bmatrix} \in R^{nr\times nr},$$

$$\hat{\mathbf{M}} = \begin{bmatrix} \int_0^1 \psi_1^2 \mathrm{d}\xi & \cdots & 0 \\ \vdots & \ddots & \vdots \\ 0 & \cdots & \int_0^1 \psi_r^2 \mathrm{d}\xi \end{bmatrix} \in R^{r\times r}$$

$$\mathbf{M}_{\eta\theta} = ml\begin{bmatrix} \hat{\mathbf{M}}_1 & \mathbf{0} & \mathbf{0} \\ \mathbf{0} & \ddots & \mathbf{0} \\ \mathbf{0} & \mathbf{0} & \hat{\mathbf{M}}_n \end{bmatrix} \in R^{nr\times n}, \ \hat{\mathbf{M}}_i = \begin{bmatrix} M_{1i} \\ \vdots \\ M_{ri} \end{bmatrix},$$

$$M_{ji} = \int_0^1 \psi_j \xi \mathrm{d}\xi + \frac{\rho_i \int_0^1 \psi_j \mathrm{d}\xi}{l}$$

Stiffness matrix:

$$\mathbf{K}_{\rho\rho} = -m\begin{bmatrix} \dot{\theta}_1^2 & \cdots & 0 \\ \vdots & \ddots & \vdots \\ 0 & \cdots & \dot{\theta}_n^2 \end{bmatrix} \in R^{n\times n},$$

$$\mathbf{K}_{\theta\rho} = 2m\begin{bmatrix} \dot{\rho}_1\dot{\theta}_1 & \cdots & 0 \\ \vdots & \ddots & \vdots \\ 0 & \cdots & \dot{\rho}_n\dot{\theta}_n \end{bmatrix} \in R^{n\times n}$$

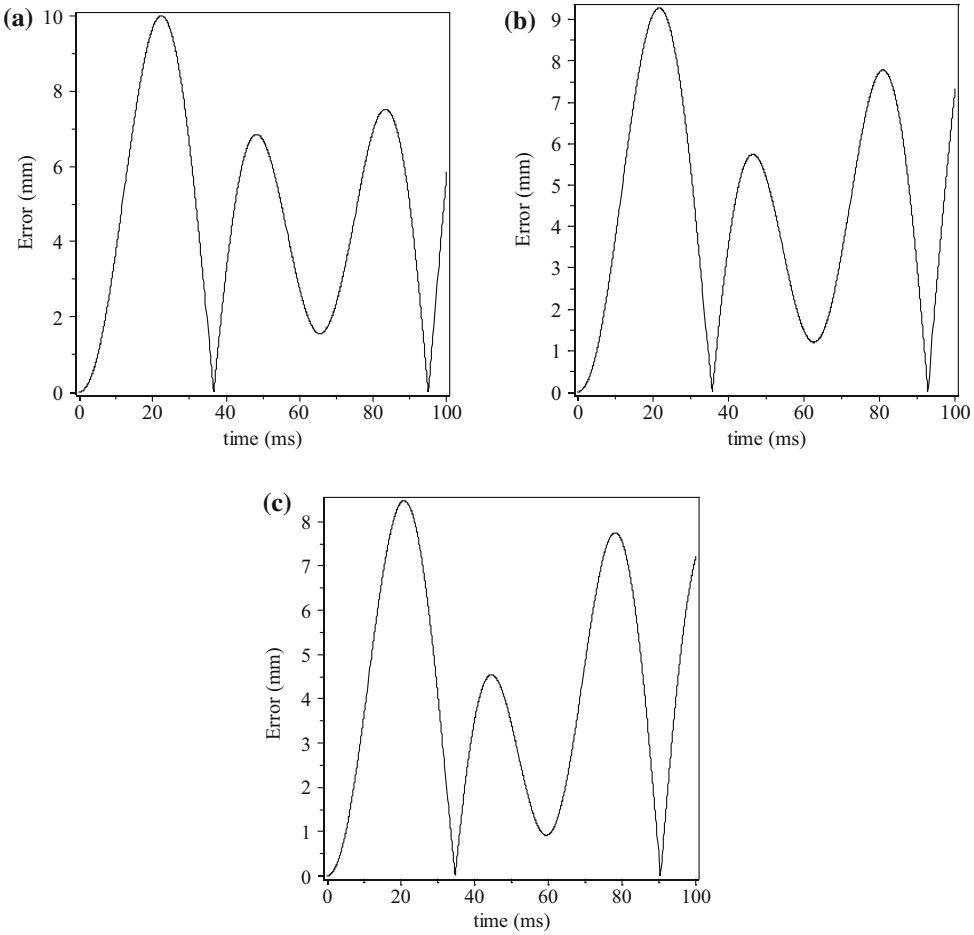

Fig. 11 Deviation magnitude. **a** 3-RPR parallel manipulator, **b** 2-RPR parallel manipulator, **c** 1-RPR serial manipulator

$$\mathbf{K}_{\eta\eta}=\frac{\mathrm{EI}}{l^3}\begin{bmatrix}\hat{\mathbf{K}} & \mathbf{0} & \mathbf{0}\\ \mathbf{0} & \ddots & \mathbf{0}\\ \mathbf{0} & \mathbf{0} & \hat{\mathbf{K}}\end{bmatrix}\in R^{nr\times nr},\hat{\mathbf{K}}=\begin{bmatrix}\int_0^1\psi_1''^2\mathrm{d}\xi & \cdots & 0\\ \vdots & \ddots & \vdots\\ 0 & \cdots & \int_0^1\psi_r''^2\mathrm{d}\xi\end{bmatrix}\in R^{r\times r},$$

Coriolis and centrifugal forces:

$$F_{c\rho}=\begin{bmatrix}(0.5\,\mathrm{ml})\dot{\theta}_1^2+\sum_{j=1}^{r}m\dot{\eta}_{1j}\dot{\theta}_1\int_0^1\psi_j\mathrm{d}\xi\\ \vdots\\ (0.5\,\mathrm{ml})\dot{\theta}_n^2+\sum_{j=1}^{r}m\dot{\eta}_{nj}\dot{\theta}_n\int_0^1\psi_j\mathrm{d}\xi\end{bmatrix},$$

$$F_{c\theta}=-m\begin{bmatrix}l\dot{\rho}_1\dot{\theta}_1+\sum_{j=1}^{r}\dot{\rho}_1\dot{\eta}_{1j}\int_0^1\psi_j\mathrm{d}\xi\\ \vdots\\ l\dot{\rho}_n\dot{\theta}_n+\sum_{j=1}^{r}\dot{\rho}_n\dot{\eta}_{nj}\int_0^1\psi_j\mathrm{d}\xi\end{bmatrix},$$

$$F_{c\eta}=\left[\dot{\rho}_1\dot{\theta}_1\int_0^1\psi_1\mathrm{d}\xi\cdots\dot{\rho}_1\dot{\theta}_1\int_0^1\psi_r\mathrm{d}\xi\cdots\dot{\rho}_n\dot{\theta}_n\int_0^1\psi_1\mathrm{d}\xi\cdots\dot{\rho}_n\dot{\theta}_n\int_0^1\psi_r\mathrm{d}\xi\right]^{\mathrm{T}}\in R^{1\times nr}$$

Jacobian matrix:

$$\mathbf{J}_{\Gamma 1}^{T}=\begin{bmatrix}\cos\theta_1 & \sin\theta_1 & \cdots & 0 & 0\\ \vdots & \vdots & \ddots & \vdots & \vdots\\ 0 & 0 & \cdots & \cos\theta_n & \sin\theta_n\end{bmatrix}\in R^{n\times 2n},$$

$$\mathbf{J}_{\Gamma 2}^{T}=\begin{bmatrix}-s2_1 & c2_1 & \cdots & 0 & 0\\ \vdots & \vdots & \ddots & \vdots & \vdots\\ 0 & 0 & \cdots & -s2_n & c2_n\end{bmatrix}\in R^{n\times 2n}$$

where $s2_i=(\rho_i+l)\sin\theta_i+\cos\theta_i\sum_{j=1}^{r}\eta_{ij}\psi_j(1)$ and $c2_i=(\rho_i+l)\cos\theta_i-\sin\theta_i\sum_{j=1}^{r}\eta_{ij}\psi_j(1)$

$$\mathbf{J}_{\Gamma 3}^{T}=\begin{bmatrix}-1 & 0 & \cdots & -1 & 0\\ 0 & -1 & \cdots & 0 & -1\\ s3_1 & -c3_1 & \cdots & s3_n & -c3_n\end{bmatrix}\in R^{3\times 2n},$$

where $s3_i = r\sin(\phi_i + \phi_p), c3_i = r\cos(\phi_i + \phi_p)$

$$\mathbf{J}_{\Gamma 4}^{T} = \begin{bmatrix} \hat{\mathbf{J}}_1 & \mathbf{0} & \mathbf{0} \\ \mathbf{0} & \ddots & \mathbf{0} \\ \mathbf{0} & \mathbf{0} & \hat{\mathbf{J}}_n \end{bmatrix} \in R^{nr\times 2n}, \hat{\mathbf{J}}_i = \begin{bmatrix} -s4_{i1} & c4_{i1} \\ \vdots & \vdots \\ -s4_{ir} & c4_{ir} \end{bmatrix},$$

$$s4_{ij} = \sin\theta_i \cdot \psi_j(1), \quad c4_{ij} = \cos\theta_i \cdot \psi_j(1)$$

References

Binaud N, Caro S, Wenger P (2011) Comparison of 3-RPR planar parallel manipulators with regard to their kinetostatic performance and sensitivity to geometric uncertainties. Meccanica 46(1):75–88

Bonev I, Zlatanov D, Gosselin C (2003) Singularity analysis of 3-DOF planar parallel mechanisms via screw theory. J Mech Des 25:573–581

Briot S, Bonev IA (2007) Are parallel robots more accurate than serial robots? CSME Trans 31(4):445–456

Briot S, Bonev IA (2008) Accuracy analysis of 3-DOF planar parallel robots. Mech Mach Theory 43(4):445–458

Briot S, Bonev I, Chablat D, Wenger P, Arakelian V (2008) Self-motions of general 3-RPR planar parallel robots. Int J Robot Res 27:855–866

Dwivedy SK, Eberhard P (2006) Dynamic analysis of flexible manipulators: a literature review. Mech Mach Theory 41:749–777

El-Khasawneh B, Alazzam A (2013) Kinematics, dynamics and vibration models for 3RPR parallel kinematics manipulator. In: ASME 2013 international mechanical engineering congress and exposition 14: vibration, acoustics and wave propagation. San Diego, California

Firoozabadi AE, Ebrahimi S, Amirian G (2015) Dynamic characteristics of a 3-RPR planar parallel manipulator with flexible intermediate links. Robotica 33:1909–1925

Guan L, Yun Y, Wang J, Wang L (2004) Kinematics of a tricept-like parallel robot. In: 2004 IEEE international conference on systems, man and cybernetics, pp 5312–5316

Kang B, Mills JK (2002) Dynamic modeling of structurally-flexible planar parallel manipulator. Robotica 20:329–339

Le TD, Kang HJ, Suh YS, Ro YS (2013) An online self-gain tuning method using neural networks for nonlinear PD computed torque controller of a 2-dof parallel manipulator. Neurocomputing 116:53–61

Merlet J-P (2006) Parallel robots, 2nd edn. Springer, Berlin, pp 4–7

Niaritsiry T-F, Fazenda N, Clavel R (2004) Study of the sources of inaccuracy of a 3 DOF flexure hinge-based parallel manipulator. In: IEEE international conference on robotics and automation, vol 4

Ogbobe P, Zhengmao Y, Jiang H, Yan C, Han J (2011) Formulation and evaluation of coupling effects between DOF motions of hydraulically driven 6 DOF parallel manipulator. Iran J Sci Technol, Trans Mech Eng 35(2):143–157

Pandilov Z, Dukovski V (2014) Comparison of the characteristics between serial and parallel robots. Acta Technica Corviniensis-Bulletin of Engineering, Tome VII, Fascicule 1 (January–March), 143–160. ISSN:2067–3809

Pashkevich A, Chablat D, Wenger P (2009) Stiffness analysis of overconstrained parallel manipulators. J Mech Mach Theory 44(5):966–982

Patel YD, George PM (2012) Parallel manipulators applications—a survey. Modern Mech Eng 2:57–64

Piras G, Cleghorn WL, Mills JK (2004) Dynamic finite-element analysis of a planar high-speed, high-precision parallel manipulator with flexible links. Mech Mach Theory 40(7):849–862

Rao SS (2007) Vibration of continuous systems. Wiley, New York

Rauf A, Kim S-G, Ryu J (2004) A new measurement device for complete parameter identification of parallel manipulators with partial pose measurements. In: The 4th Chemnitz parallel kinematics seminar. Chemnitz, Germany, pp 89–106

Seifried R, Burkhardt M, Held A (2013) Trajectory control of serial and parallel flexible manipulators using model inversion. Multibody Dyn 28:53–75

Song J-I, Mou J, King C (1999) Error modeling and compensation for parallel kinematic machines. In: Parallel kinematic machines, advanced manufacturing series. Springer, London, pp 171–187

Staicu S (2009a) Power requirement comparison in the 3-RPR planar parallel robot dynamics. Mech Mach Theory 44(5):1045–1057

Staicu S (2009b) Inverse dynamics of the 3-PRR planar parallel robot. Robot Auton Syst 57(5):556–563

Staicu S (2009c) Power requirement comparison in the 3-RPR planar parallel robot dynamics. Mech Mach Theory 44:1045–1057

Staicu S (2013) Joint forces in dynamics of the 3–RRR planar parallel robot. Int J Mech Robot 1(4):283–300

Staicu S, Chablat D (2012) Internal joint forces in dynamics of a 3-PRP planar parallel robot. Proc Rom Acad, Ser A 13(3):235–242

Staicu S, Carp-Ciocardia DC, Codoban A (2007) Kinematics modelling of a planar parallel robot with prismatic actuators. UPB Sci Bull, Series D 69:3–14

Sudhakar U, Srinvas J (2013) A stiffness index prediction approach for 3-RPR planar parallel linkage. Int J Eng Res Technol 2(9):2747–2751

Tsai LW, Joshi S (2001) Comparison study of architectures of four 3 degree-of-freedom translational parallel manipulators. In: Proceedings of the 2001 IEEE Seoul, Korea, international conference on robotics and automation

Viliani NS, Zohoor H, Kargarnovin MH (2012) Vibration analysis of a new type of compliant mechanism with flexible-link using perturbation theory. Math Prob Eng 1–19, Article ID 857064. doi:10.1155/2012/857064

Wavering AJ (1999) Parallel kinematic machine research at NIST: past, present and future. In: Boër CR, Molinari-Tosatti L, Smith KS (eds) Parallel kinematic machines, advanced manufacturing series. Springer, Berlin, pp 17–31

Williams RL, Joshi AR (1999) Planar parallel 3-RPR manipulator. In: Proceedings of the sixth conference on applied mechanisms and robotics, Cincinnati OH

Wu J, Wang JS, Wang LP, You Z (2010a) Performance comparison of three planar 3-DOF parallel manipulators with 4-RRR, 3-RRR and 2-RRR structures. Mechatronics 20(4):510–517

Wu J, Wang JS, Wang LP (2010b) A comparison study of two planar 2-DOF parallel mechanisms: one with 2-RRR and the other with 3-RRR structures. Robotica 28(10):937–942

Wu J, Wang JS, You Z (2011) A comparison study on the dynamics of planar 3-DOF 4-RRR, 3-RRR and 2-RRR parallel manipulators. Robot Comput Integr Manuf 27:150–156

Wu J, Li T, Wang JS, Wang LP (2013) Performance analysis and comparison of planar 3-DOF parallel manipulators with one and two additional branches. J Intell Robot Syst 72(1):73–82

Zhang D, Gao Z, Su X, Li J (2012) A comparison study of three degree-of-freedom parallel robotic machine tools with/without actuation redundancy. Int J Comput Integr Manuf 5(3):230–247

Zhao Y, Gao F (2009) Dynamic performance comparison of the 8PSS redundant parallel manipulator and its non-redundant counterpart—the 6PSS parallel manipulator. Mech Mach Theory 44(9):991–1008